AD-A137 971 ANALYSIS OF MICROSTRUCTURE AND STRENGTHENING MECHANISMS 1/1
IN LASER SURFACE.. (U) OREGON GRADUATE CENTER BEAVERTON
W E WOOD 22 DEC 83 ARO-16916-7-MS DAAG29-80-K-0023
UNCLASSIFIED F/G 11/6 NL

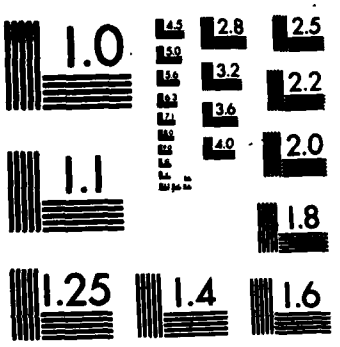

ANALYSIS OF MICROSTRUCTURE AND STRENGTHENING MECHANISMS IN LASER SURFACE ALLOYED Fe-Cr AND Fe-C-Cr ALLOY SYSTEMS

FINAL REPORT

WILLIAM E. WOOD

DECEMBER 22, 1983

U. S. ARMY RESEARCH OFFICE

CONTRACT/GRANT NUMBER DAAG29-80-K-0023

OREGON GRADUATE CENTER

SECURITY CLASSIFICATION OF THIS PAGE (When Data Entered)

REPORT DOCUMENTATION PAGE

READ INSTRUCTIONS BEFORE COMPLETING FORM

1. REPORT NUMBER: 16916-MS	2. GOVT ACCESSION NO.
3. RECIPIENT'S CATALOG NUMBER	
4. TITLE (and Subtitle): ANALYSIS OF MICROSTRUCTURE AND STRENGTHENING MECHANISMS IN LASER SURFACE ALLOYED Fe-Cr AND Fe-C-Cr ALLOY SYSTEMS	5. TYPE OF REPORT & PERIOD COVERED: Final Report, July 8, 1980 - Oct. 31, 1983
	6. PERFORMING ORG. REPORT NUMBER
7. AUTHOR(s): William E. Wood	8. CONTRACT OR GRANT NUMBER(s): DAAG29-80-K-0023
9. PERFORMING ORGANIZATION NAME AND ADDRESS: Oregon Graduate Center, 19600 N.W. Walker Road, Beaverton, OR 97006	10. PROGRAM ELEMENT, PROJECT, TASK AREA & WORK UNIT NUMBERS
11. CONTROLLING OFFICE NAME AND ADDRESS: U. S. Army Research Office, Post Office Box 12211, Research Triangle Park, NC 27709	12. REPORT DATE: December 22, 1983
	13. NUMBER OF PAGES: 23
14. MONITORING AGENCY NAME & ADDRESS(if different from Controlling Office)	15. SECURITY CLASS. (of this report): Unclassified
	15a. DECLASSIFICATION/DOWNGRADING SCHEDULE

16. DISTRIBUTION STATEMENT (of this Report)

Approved for public release; distribution unlimited.

17. DISTRIBUTION STATEMENT (of the abstract entered in Block 20, if different from Report)

18. SUPPLEMENTARY NOTES

THE VIEW, OPINIONS, AND/OR FINDINGS CONTAINED IN THIS REP[illegible] ARE THOSE OF THE AUTHOR[illegible] AND SHOULD NOT BE CONSTRUED AS AN OFFICIAL DEPARTMENT T[illegible] POLICY, OR D[illegible] UNLESS SO DESIGNATED BY OTHER DOCUMENTATION.

19. KEY WORDS (Continue on reverse side if necessary and identify by block number)

Laser alloying, Fe-Cr, Fe-Cr-C, Microstructural Analysis

20. ABSTRACT (Continue on reverse side if necessary and identify by block number)

The effects of rapid melting and subsequent quenching on the solidification behavior and solid state transformation structures of laser surface alloyed Fe-Cr, Fe-Ni, Fe-Cr-Ni and Fe-C-Cr systems were investigated as functions of composition (0-50%Cr, 0-20%Ni, 0-20%Cr/Ni, 0-1%C) and cooling rate ~~(10^3-10^6°C/s)~~. The microstructures were characterized by optical, scanning and thin foil transmission electron microscopy. The effects of laser parameters (laser power, beam size and scan rate) and coating variables (composition, thickness and morphology) on the penetration depth and melt width were also evaluated. →

DD FORM 1 JAN 73 1473 EDITION OF 1 NOV 65 IS OBSOLETE

Unclassified

SECURITY CLASSIFICATION OF THIS PAGE (When Data Entered)

20. (cont.)

The microstructures of Fe-Cr alloys were ferritic in nature, irrespective of the composition (0-50%Cr) and cooling rate (~~10^3-10^6°C/s~~). The transformation structures of Fe-5%Ni and Fe-6%Cr-2%Ni alloys exhibited a mixture of martensite and ferrite. The transformation structures of Fe-C-Cr alloys were studied as functions of the carbon (0.2-1.0%C) and chromium contents (0-40%Cr). The alloys containing up to 10%Cr exhibited a martensitic structure with fine precipitates of M_3C carbide and small amounts of retained austenite. The 20%Cr alloys consisted of duplex austenite/ferrite structures. The morphology and substructure of austenite were a function of the carbon content. Carbide precipitation was identified only in a 1.0%C alloy. The 40%Cr alloys were ferritic and the morphology changed from equiaxed grains to regular cells with increasing carbon content. Significant amounts of $M_{23}C_6$ carbide were also observed in these alloys.

The rapid solidification effects including the retention of supersaturated austenite, lack of carbide precipitation and the morphology of phases are discussed as functions of alloy content and cooling rate.

TABLE OF CONTENTS

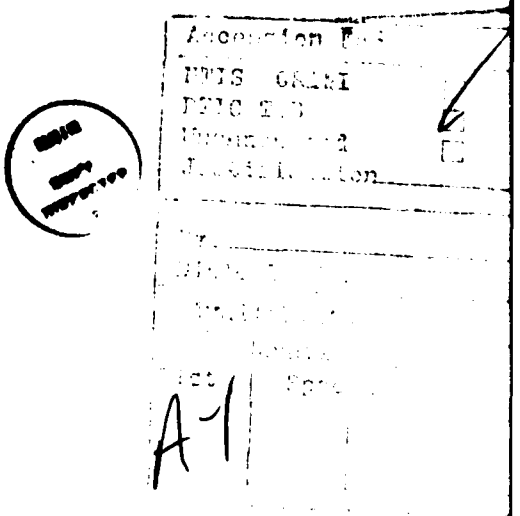

LIST OF TABLES AND FIGURES

I. ABSTRACT

The effects of rapid melting and subsequent quenching on the solidification behavior and solid state transformation structures of laser surface alloyed Fe-Cr, Fe-Ni, Fe-Cr-Ni and Fe-C-Cr systems were investigated as functions of composition (0-50%Cr, 0-20%Ni, 0-20%Cr/Ni, 0-1%C) and cooling rate (10^3-10^6°C/s). The microstructures were characterized by optical, scanning and thin foil transmission electron microscopy. The effects of laser parameters (laser power, beam size and scan rate) and coating variables (composition, thickness and morphology) on the penetration depth and melt width were also evaluated.

The microstructures of Fe-Cr alloys were ferritic in nature, irrespective of the composition (0-50%Cr) and cooling rate (10^3-10^6°C/s). The transformation structures of Fe-5%Ni and Fe-6%Cr-2%Ni alloys exhibited a mixture of martensite and ferrite. The transformation structures of Fe-C-Cr alloys were studied as functions of the carbon (0.2-1.0%C) and chromium contents (0-40%Cr). The alloys containing up to 10%Cr exhibited a martensitic structure with fine precipitates of M_3C carbide and small amounts of retained austenite. The 20%Cr alloys consisted of duplex austenite/ferrite structures. The morphology and substructure of austenite were a function of the carbon content. Carbide precipitation was identified only in a 1.0%C alloy. The 40%Cr alloys were ferritic and the morphology changed from equiaxed grains to regular cells with increasing carbon content. Significant amounts of $M_{23}C_6$ carbide were also observed in these alloys.

The rapid solidification effects including the retention of supersaturated austenite, lack of carbide precipitation and the morphology of phases are discussed as functions of alloy content and cooling rate.

II. INTRODUCTION

In recent years, significant advances have been made utilizing high energy density focussed beams for materials processing. Among the potential applications, laser surface alloying is one of the last to be developed due to the complexity of the microstructural features developed and the wide range of solidification and solid-state transformation features produced or suppressed. Laser surface alloying basically consists of applying either during alloying or prior to laser processing a thin coating onto the surface of a substrate and then scanning the surface with a laser beam to produce melting and alloying. This process can produce high melting efficiency, rapid solidification, minimum distortion, limited heat affected zones, formation of metastable phases, fine grain size, and other tailored microstructural features.

In order to exploit the potential mechanical property advantages of laser processed surfaces, it is essential to develop detailed understandings of the microstructures, solidification rates, and laser beam parameters that collectively control the resulting microstructure as a function of process parameters. Development of unusually fine structures increased solid solubilities of nonequilibrium crystalline and amorphous phases, modified segregation patterns and high defect concentrations in rapidly quenched metals and alloys have stimulated efforts among investigators to develop theories to explain various phenomena observed. While the microstructures of rapidly solidified splat quenched alloys have been studied in detail, little attention has been directed at the allied process of laser melting at somewhat slower solidification and cooling rates.

This present program was undertaken to study the effects of laser melting and quenching on the solidification behavior and transformation

structures of laser surface alloyed Fe-Cr and Fe-Cr-C systems as a function of composition (5-50%Cr, 0-1%C) and cooling rate (10^3-10^6°C/s). The Fe-Cr and Fe-Cr-C systems were selected due to the extensive literature available and the practical significance of these systems.

The key variables were laser power, beam size, scan rate, coating composition, coating thickness and coating morphology. Basically, increasing the laser power increases melt penetration, may or may not ensure uniform mixing, can introduce surface rippling, increases the heat affected zone size, may drastically alter the shape of the fusion zone, and sometimes increases cracking tendencies. Focussing the laser beam ensures maximum power density but narrows the melting width, while increasing the beam diameter increases the width of the fusion zone but reduces intensity of the input, and, therefore, diminishes melt penetration.

The following sections summarize briefly some of the procedures and results that were obtained during this investigation. The information has been published in both journals and as a thesis.

III. EXPERIMENTAL METHODS

The substrate materials in this investigation range from electrolytically pure iron to commercial quality plain carbon steels with carbon contents varying from .2 to 1%. All materials were vacuum degassed prior to laser processing. Standard electrodepositing conditions were utilized for a deposition of chromium or nickel plus chromium sequentially. Samples were again degassed to a minimum of 10^{-7} torr at 400°F prior to laser processing. Failure to do this resulted in gross porosity in the laser processed zone.

A Spectra-Physics Model 971 CO_2 gas transport laser was utilized. This laser is capable of producing up to 1500 watts of continuous infrared laser radiation with a wavelength of 10.6μ. Cooling rates in this program were calculated based upon both heat transfer models as well as measurement of solidification structures and predictions of the corresponding solidification cooling rates using standard solidification practice. Both energy and wavelength dispersive x-ray microprobe analysis were used to determine the composition of the surface alloys produced. This produced excellent agreement with the calculated results based upon dilution measurements. Microscopy consisted of optical, scanning and transmission electron microscopy of laser processed zones. Standard metallographic and microscopy techniques were employed to prepare the samples.

The bulk of the work was carried out with a fixed laser beam configuration under which the workpiece was traversed at appropriate scan rates to produce either a single pass or multiple pass with variable overlap. The interaction of time, the laser power density, the total power, and the position of the workpiece with respect to the focal point of the laser beam were all varied as well as the substrate and the coating composition and thickness.

During the later stages of this program, a laser rastering system was designed and fabricated which would allow rapid oscillation of the laser beam. The rastering system consisted of a polygonal 20-facet rotating mirror. Each facet was approximately 1 inch across and the polygon was approximately 6 inches in diameter. The beam, after passing through the focussing lens, was deflected by 90° to the substrate work surface. A 2-1/2" focal length lens was used for all studies, which with the particular rastering system, produced a rastered melt zone width of approximately 8mm for this investigation. Thus, using this relatively simple rastering system and a 1500 watt CO_2 laser, 1/4 inch wide melt width could readily be achieved under single pass operations. This greatly extends the applicability of what is now intermediate size laser systems for more efficient processing of larger surface areas.

IV. SUMMARY OF RESULTS

As the laser beam power is increased, the penetration depth increases linearly with power, but the melt width remains rather insensitive due to the overall power density distribution of the highly focussed beam. Under deep penetration conditions, keyholing develops as under electron beam conditions. The influence of power density and scan rate is shown with respect to the melt depth in Figure 1. Similarly, the influence interaction time or travel speed as represented by inches per minute of tr l versus the output power in watts may rarely be seen, Figure 2. A key relationship is the position of the workpiece with respect to the focussed laser beam. Figure 3 shows that by maintaining a focal point slightly into the work surface, that a wider range of variation is allowed without having significant influences on the penetration depth. While in this program the Fe-Cr system was nearly studied in detail, some initial work was carried out using sequentially deposited nickel and chromium coatings as opposed to either nickel or chromium. The influence of the dual coating is shown in Figure 4, where for the same total coating thickness, the dual coating has a much higher penetration melt depth than either of the single coatings. While noted in this investigation, the program did not pursue the investigation of this phenomenon, but it is included in order to show the unexpected variations that can occur during laser material interaction studies. Also noted in passing was the effect of black chrome versus bright chrome and chromium-iron co-deposition on the penetration for various scan rates. Clearly, at relatively deep penetrations and correspondingly slow workpiece scan rates, there is a significant influence of the chromium deposit on the resulting melt depth. This effect is reduced at smaller penetrations produced by more

rapid scanning. This again points to the difficulty of generalizing on particular laser processing data and results without a more detailed understanding of the specific interactions of the beam with the surfaces and the coatings.

In order to vary the chromium concentrations in the laser process zone, both the melt depth as well as the initial plating thickness were varied. In all cases, the theoretical calculation of the percent chromium as a function of cross sectional area agreed excellently with x-ray analysis based on the knowledge of the plating thickness, scan rate, power density and particular electrodeposited coating. The penetration depth, solidification rate and resulting microstructures can be predicted as a result of this portion of the investigation.

Both one and three-dimensional heat flow models for a directed high energy source were studied in relationship to the observed dendritic arm spacing and resulting solidification calculations based upon the relationship that the dendrite arm spacing is equivalent to $(60)(r)^{-0.41}$, where r is the cooling rate in degrees C per second. In general, the theoretical cooling rate models worked well when the melt depth was 500μ or less. This corresponded to a semi-circular melt zone with very uniform composition. However, on a deeper penetration, which tended to produce a keyholing effect, the existing heat flow models tended to underestimate the solidification rates obtained in this program. By measuring the cell spacings together with the penetration depth, the solidification will be obtained as a function of melt depth. These results are summarized in Figures 7 and 8, in which the cell structure is shown as a function of melt depth and the cell spacings as a function of penetration depth together with the theoretical cooling rate from heat flow models. In this program, the cell spacing

obtained ranged from 1000 Å to as much as 4μ, depending upon melting conditions. The availability of this data together with laser melting parameters allows the solidification rate penetration depth and composition all to be predicted based upon the laser alloying parameters and coating thicknesses. Thus, these data act as guidelines for establishing predicted laser operating parameters for surface alloying of chromium.

An important aspect of laser alloying is the profile of the melt zone as a function of power density and interaction time, since it can significantly influence the overall chemical homogeneity of the melt depth. These data are summarized in Figures 9 and 10, where it is seen that for relatively shallow semi-circular melts, an extremely uniform melt composition is achieved. However, the overall melt depth is shallow and as the melt depth becomes more and more penetrating, the geometry changes and a sharp gradient can be developed between the near surface and the near interface zones of the melt. While the overall depth to which a relatively uniform concentration can be achieved is increased by deeper melting, the gradient can produce significantly different structures from the top to the bottom zone. This is illustrated in Figure 10, where the bottom of the melt zone has reduced chromium concentration, which results in a γ to α transformation, whereas the upper portion of the melt zone with increased chromium is within the ferritic zone of the iron-chrome binary phase diagram. This phenomena, if taken advantage of, should result in the ability to produce a graded chemistry, graded microstructure from the top to the bottom or at the interface zone to intentionally produce compatible surface and substrate properties. However, if not taken into account, significantly different chemistries and structures may be developed beyond that predicted from uniform chemistry mixing assumptions.

A general summary of the microstructures produced during this laser alloying program as a function of chromium and carbon content is shown in Table I. Generally, all structures showed retained austenite films commonly observed in quenched martensitic structures. Shown in parenthesis in Table I are the equilibrium phases expected for each composition. Of particular note in the results is that for 20%Cr, there was no evidence of carbides formed with either .2C or .5C. With only 10%Cr, it was impossible to suppress the formation of ε-carbide under any quench rates utilized in this investigation. For the 40%Cr alloys, the morphology of the ferrite was a function of the carbon content. At low carbon contents, the ferrite was equiaxed, while at the intermediate and higher carbon concentrations, a cellular solidification morphology was observed with extensive precipitation of chromium-carbides at intercellular boundaries. At more rapid solidification rates than obtained in this present work, which can develop additional undercooling, the alloy may solidify as a homogeneous solid solution rather than a cellular solidification morphology.

For the .2C-20%Cr alloy, whose phase diagram is shown in Figure 11, a metastable duplex ferrite/austenite structure was developed under certain laser processing conditions that exhibited a minimum solidification and cooling rate. Results are shown in Figure 12, where for a single scan melt depth of 600μ, an acicular austenite needle structure and a ferrite matrix was obtained. If multiple pass surface melting is carried out, the adjacent passes will transform the retained austenite to a martensitic lath structure. However, if the melting depth is decreased, and thus the solidification and cooling rates increased, the multiple adjacent passes will not result in the transformation of metastable austenite, but rather result in the entire area consisting of duplex metastable ferritic and acicular austenitic microstructure.

Formation of this metastable austenite phase depends strongly upon the cooling rate as well as the chromium and carbon concentrations. Micrographs of the typical retained austenite pattern as well as ε-carbide in .2C-5Cr alloys are shown in Figure 13 and the transmission microscopy analysis of a metastable acicular austenite and ferritic matrix is represented in Figure 14. Finally, for comparison, at high chromium concentrations and increasing carbon concentrations, duplex austenite ferrite structures are obtained which show a significantly different morphology than the thin acicular austenite developed with lower carbon concentrations.

These results show that the amount, the distribution, and the stability of the metastable austenite in a ferritic matrix may be adjusted by laser parameters and chemical compositions. Also, that the presence, morphology, and extent of carbides present may also be controlled by similar parameters. Based upon available literature shown in Figure 16, increasing the solidification rate to that approaching 10^7 or 10^8°C/s should result in a fully austenitic microstructure at the higher carbon levels.

In order to evaluate this possibility, a laser rastering system was designed and built during this program to allow very high laser beam sweep rates. While this system is currently producing melt widths of over 8mm due to the width of the raster beam, the present study has not yet been able to optimize the laser and substrate parameters to produce exceedingly thin surface melts. Thus, the present investigation was limited to relatively thick 500μ deep laser rastered melt zones in order to produce a controlled surface melting interaction. Work is continuing beyond this program to refine the rastered parameters, together with beam quality and substrate movement to try to produce solidification rates an order of magnitude higher than those achieved to date. This should result in secondary dendrite arm

spacings of less than .1μ and cooling rates on the order of 10^7°C/s while allowing a relatively wide process zone to facilitate microscopy analysis.

V. CONCLUSIONS

The principal conclusions of this investigation into the effects of rapid melting and subsequent quenching on the solidification behavior and solid-state transformation structures of laser surface alloyed Fe-Cr and Fe-Cr-C systems are as follows:

1. All laser parameters, including variables, must be closely controlled in order to obtain consistent results. Deviations in some parameters can result in significant changes in the resulting melt depth and solidification profiles.

2. For this investigation, cooling rates obtained were between 10^3 and 10^6°C/s.

3. The overall chemical uniformity of the melted zone is a strong function of the melt profile. This can allow tailored created compositions and microstructures to be designed for specific applications.

4. Unique microstructures containing metastable austenite in a ferritic matrix were observed, particularly in the Fe-20%Cr-C system. The substructure and morphology of the austenite in each case was a function of the carbon content and chromium content together with the solidification and cooling rate. Extensions of this work and to higher solidification rates should allow the development of additional amounts of metastable austenite phase being retained and the further suppression of carbide precipitation.

5. This program has demonstrated that the fundamental laser materials interactions solidification research can be carried out on a 1500 watt CO_2 laser system and very large systems are not required to generate the structures, including metastable phases and multiple precipitation reactions.

Table I.

Alloy System Cr Content	Fe-0.2%C-Cr	Fe-0.5%C-Cr	Fe-1.0%C-Cr
10%	Lath martensite + M_3C carbide + Retained austenite	Lath martensite + M_3C carbide + Retained austenite	Plate martensite Retained austenite
	(Ferrite + $M_{23}C_6$)	(Ferrite + M_7C_3 + $M_{23}C_6$)	(Ferrite + M_7C_3)
20%	Ferrite + Austenite	Ferrite + Austenite	Austenite + $M_{23}C_6$ Ferrite
	(Ferrite + $M_{23}C_6$)	(Ferrite + $M_{23}C_6$)	(Ferrite + $M_{23}C_6$)
40%	Equiaxed Ferrite + $M_{23}C_6$	Cellular Ferrite + $M_{23}C_6$	Cellular Ferrite + $M_{23}C_6$
	(Ferrite + $M_{23}C_6$)	(Ferrite + $M_{23}C_6$),	(Ferrite + $M_{23}C_6$)

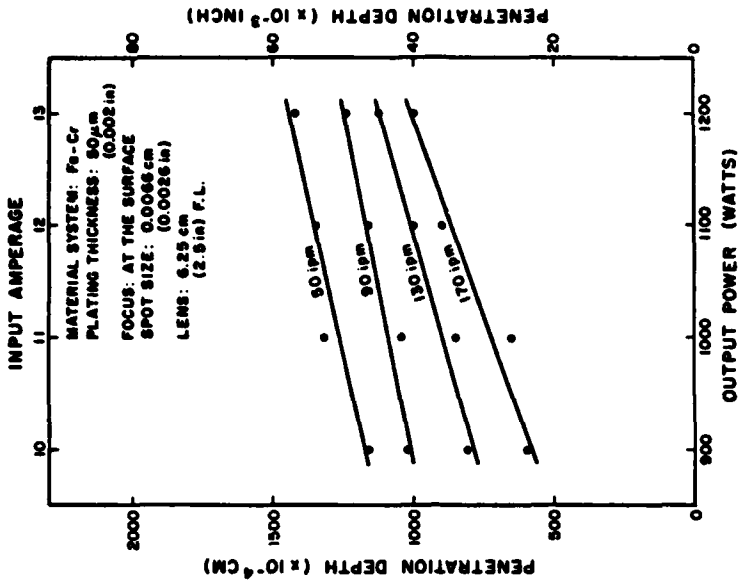

Figure 2. EFFECT OF LASER POWER ON MELT PENETRATION OF Fe-Cr ALLOYS.

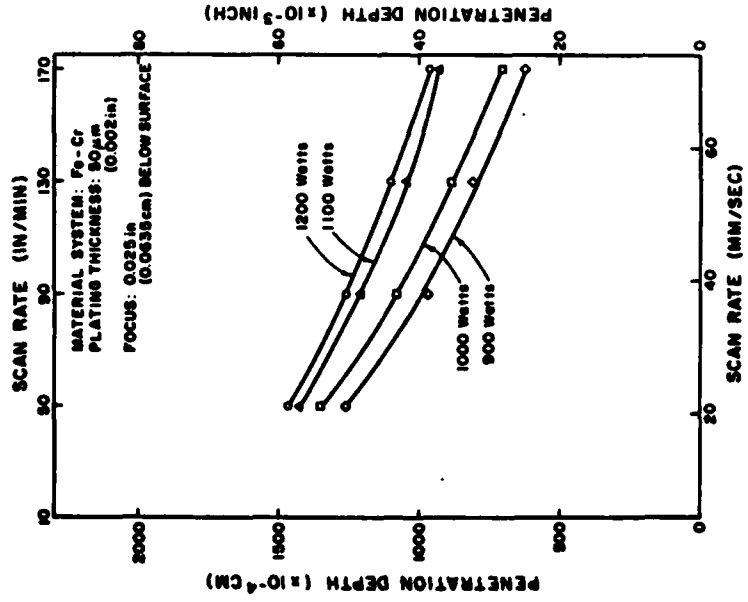

Figure 1. EFFECT OF SCAN RATE ON MELT PENETRATION OF Fe-Cr ALLOYS.

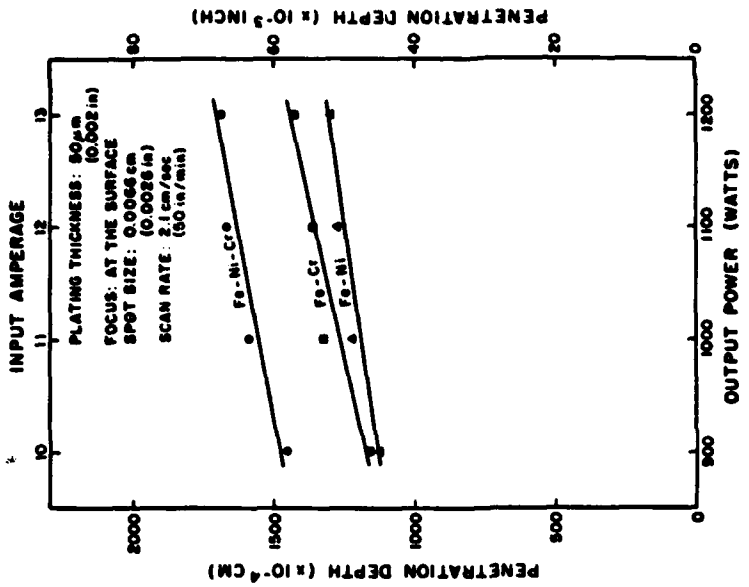

Figure 4. EFFECT OF COATING COMPOSITION ON MELT PENETRATION OF Fe-Cr, Fe-Ni AND Fe-Cr-Ni ALLOYS FOR VARIOUS LASER POWERS.

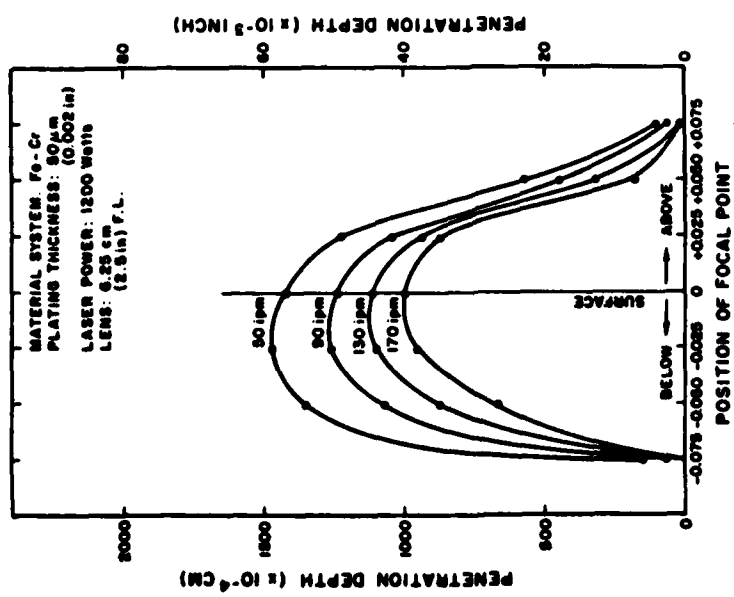

Figure 3. EFFECT OF FOCAL POSITION ON MELT PENETRATION OF Fe-Cr ALLOYS.

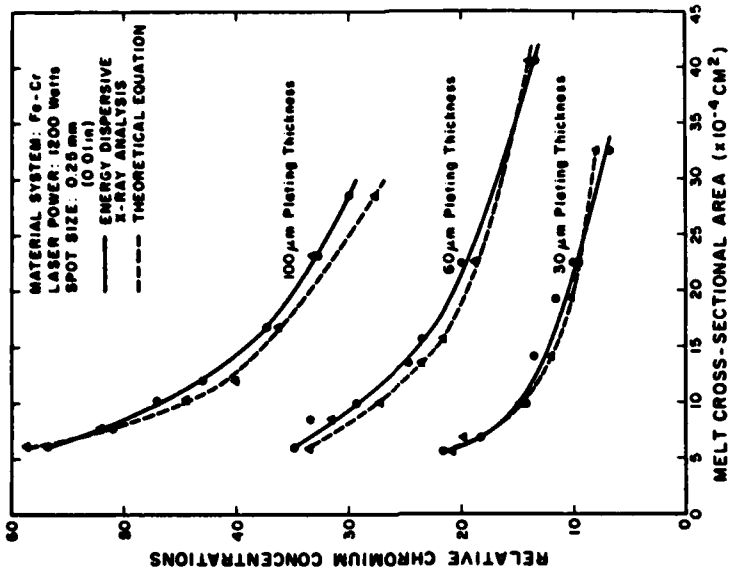

Figure 6. EFFECT OF COATING THICKNESS AND FUSION ZONE CROSS-SECTIONAL AREA ON THE ALLOY CONTENT OF FUSION ZONE.

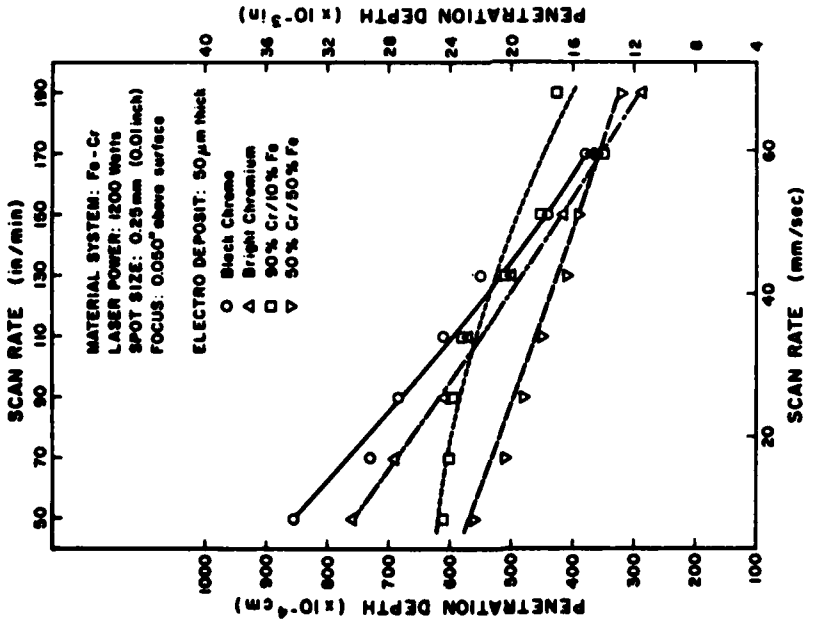

Figure 5. EFFECT OF COATING MORPHOLOGY ON MELT PENETRATION OF Fe-Cr ALLOYS.

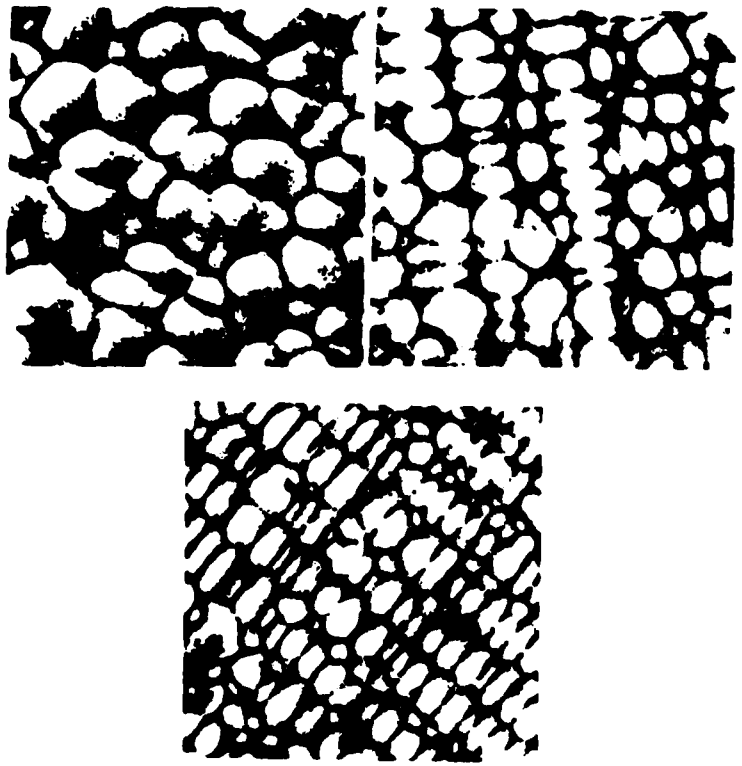

Figure 7. SCANNING ELECTRON MICROGRAPHS SHOWING THE SOLIDIFICATION STRUCTURES OF Fe-1.0%C-Cr ALLOYS WITH PENETRATION DEPTHS OF

a) 1000μm, b) 790μm, c) 700μm.

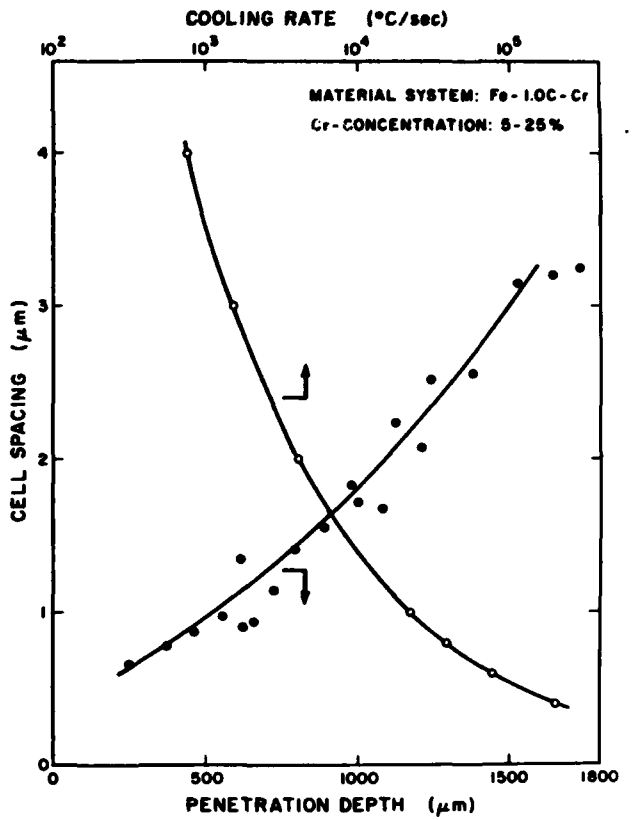

Figure 8. EFFECT OF PENETRATION DEPTH ON THE CELL SPACING OF SOLIDIFICATION STRUCTURES OF Fe-C-Cr ALLOYS.

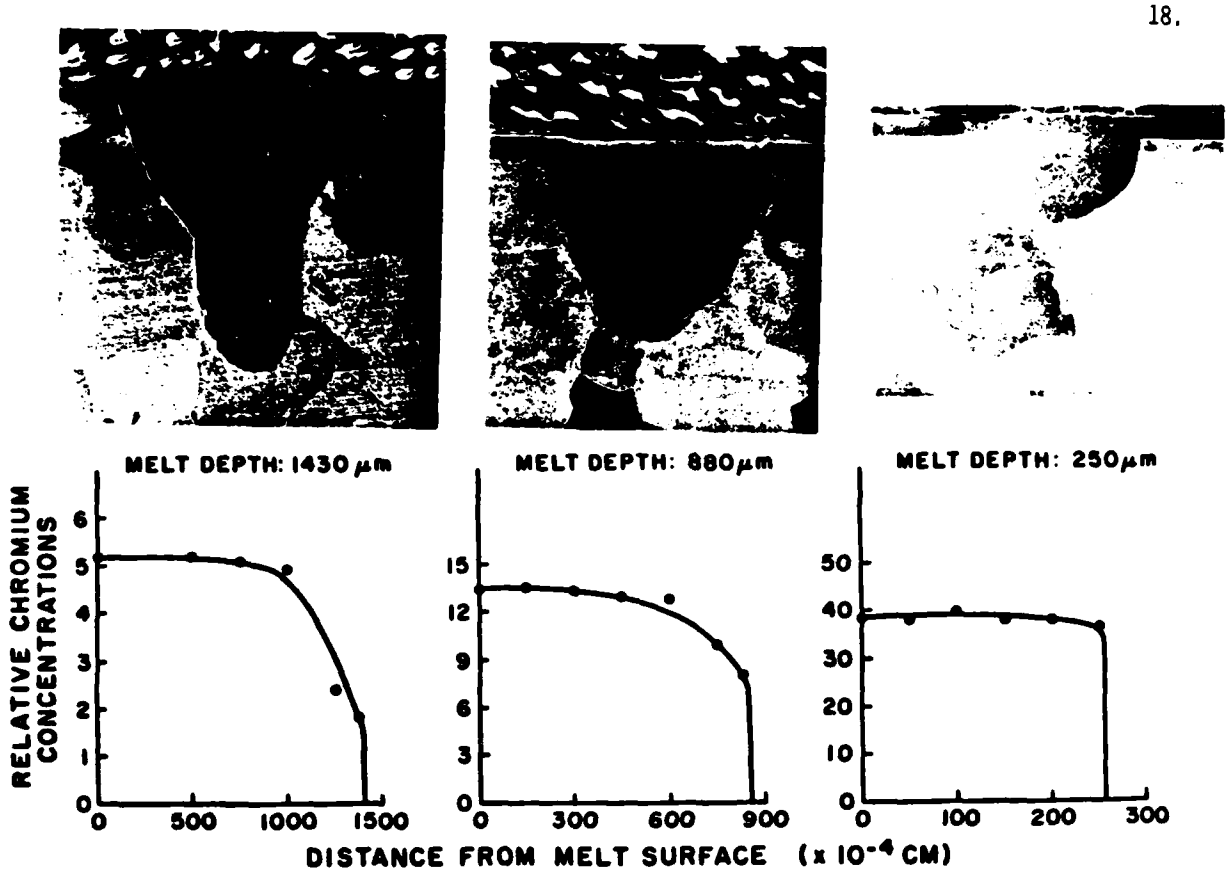

Figure 9. **Composition uniformity of fusion zone as a function of fusion zone shape**

Figure 10. LIGHT MICROGRAPH OF A Fe-Cr ALLOY SHOWING THE VARIATION IN THE MORPHOLOGY OF FERRITE FROM THE BOTTOM TO THE TOP SURFACE OF FUSION ZONE AS A FUNCTION OF CHROMIUM CONTENT. MAGNIFICATION: 160x.

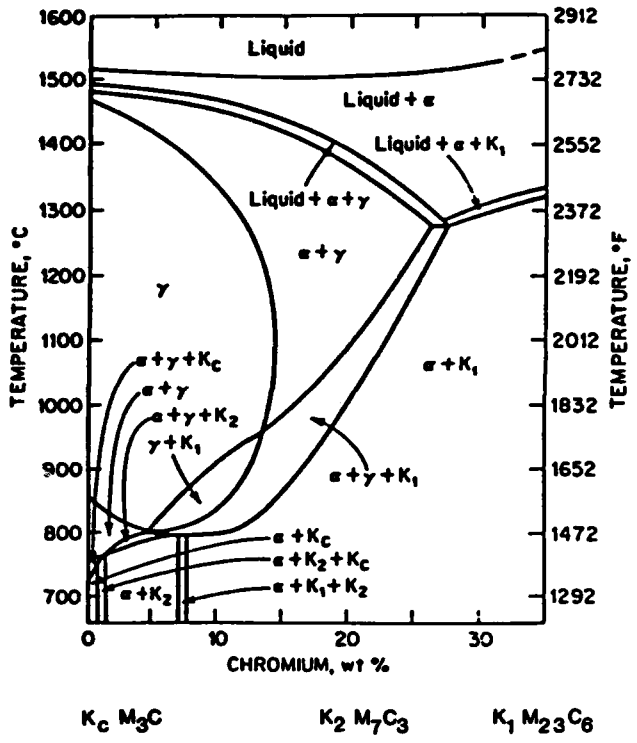

Figure 11. THE Fe-0.2%C-Cr PHASE DIAGRAM.

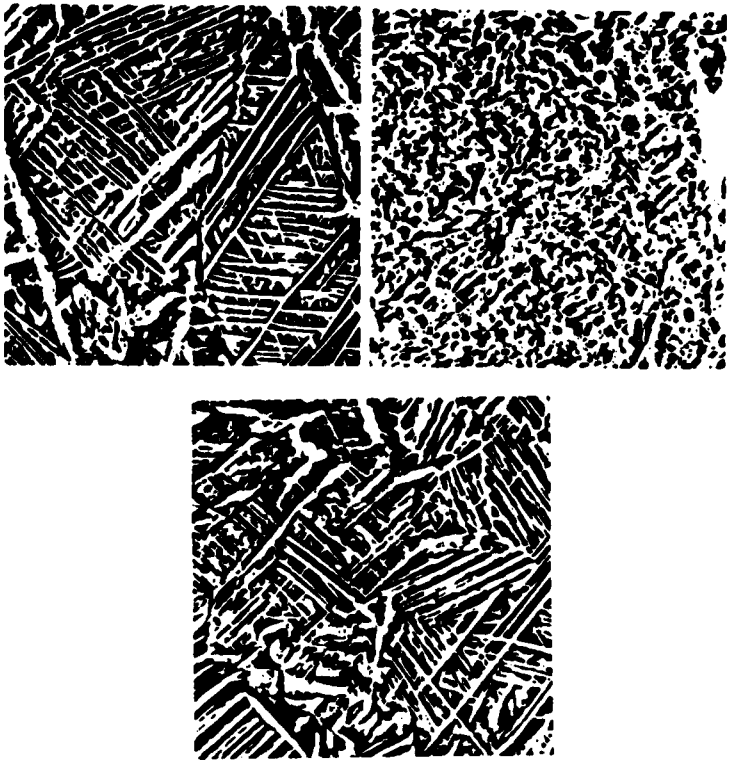

Figure 12. SCANNING ELECTRON MICROGRAPHS SHOWING THE MICROSTRUCTURES OF LASER PROCESSED Fe-0.2%C-20%Cr ALLOYS

a) SINGLE SCAN (PENETRATION DEPTH: 600μm)
b) MULTIPLE SCAN (PENETRATION DEPTH: 600μm)
c) MULTIPLE SCAN (PENETRATION DEPTH: 120μm)

MAGNIFICATION: 1000x.

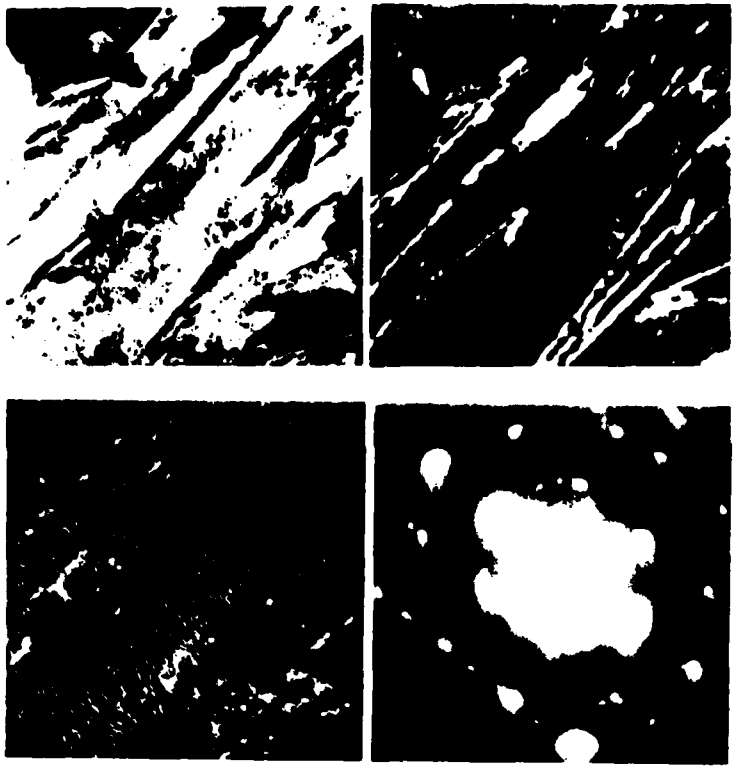

Figure 13. TRANSMISSION ELECTRON MICROGRAPHS OF LASER PROCESSED Fe-0.2%C-5%Cr ALLOY (PENETRATION DEPTH: 1500μm)

a) BF, b) DF SHOWING RETAINED AUSTENITE
c) DF SHOWING ε-CARBIDE, d) SAD PATTERN

MAGNIFICATION: 18,000x.

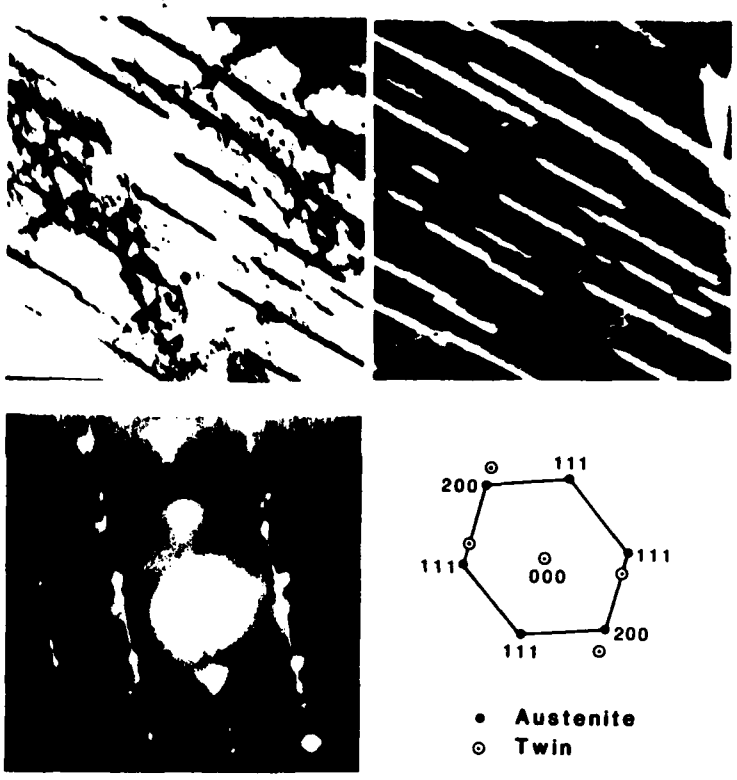

Figure 14. TRANSMISSION ELECTRON MICROGRAPHS OF LASER PROCESSED Fe-0.2%C-20%Cr ALLOY (PENETRATION DEPTH: 120μm, MULTIPLE SCAN)

a) BF, b) DF SHOWING THE AUSTENITIC NEEDLES,
c) SAD PATTERN, d) ANALYSIS OF SAD

MAGNIFICATION: 18,000x.

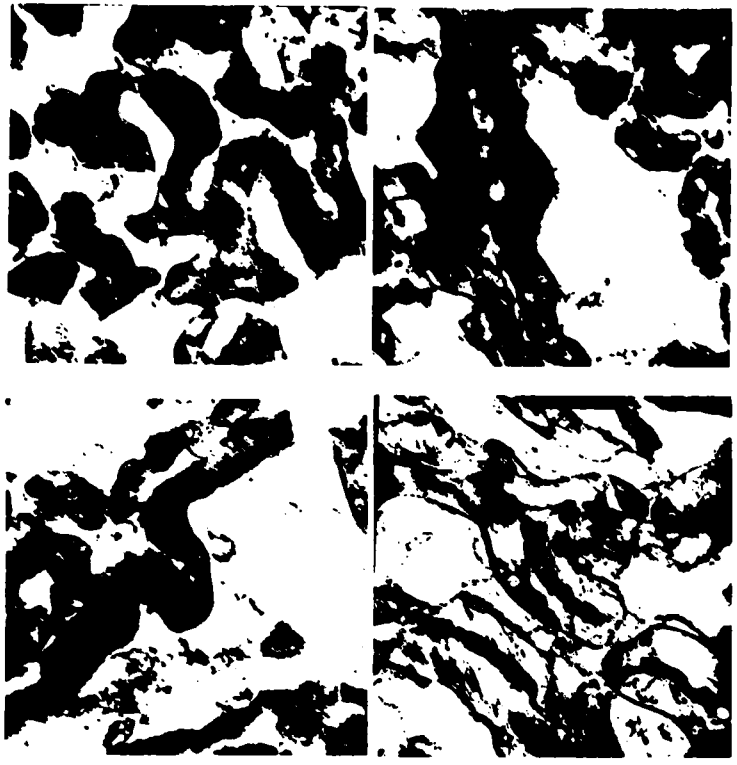

Figure 15. TRANSMISSION ELECTRON MICROGRAPHS OF LASER PROCESSED Fe-0.5%C-20%Cr ALLOY SHOWING THE AUSTENITE/FERRITE STRUCTURES (PENETRATION DEPTH: 210μm). MAGNIFICATION: 18,000x.

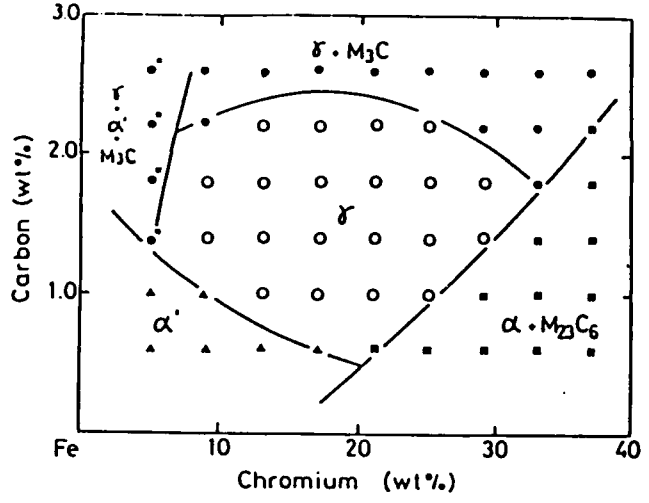

Figure 16. A NON-EQUILIBRIUM DIAGRAM FOR "SPLAT-COOLED" Fe-C-Cr ALLOYS [AFTER INOUE ET AL (100)].

LIST OF PUBLICATIONS

Laser Surface Alloying of Metallic Materials, W. Wood and J. Johnsen, poster presentation at Pacific Northwest Metals & Minerals Conference, Seattle, WA, May 1980 (invited presentation). (Presentation only--no paper)

Optimization of Process Variables in Laser Surface Alloying Applications, P. A. Molian and W. E. Wood, presented at 1981 Pacific Northwest Metals & Minerals Conference, Portland, OR, April 27-29, 1981. (Presentation only--no paper)

Microstructural Characterization of Laser Surface Alloyed Iron, P. A. Molian, J. L. Johnsen and W. E. Wood, SME Lasers in Manufacturing Conference, Nov. 11-13, 1980, Los Angeles, CA; 1981 SME Manufacturing Engineering Transactions/ 9th NAMRC (North American Manufacturing Research Conference) Proceedings, Society of Manufacturing Engineers, May 1981, pp. 1-7.

Microstructures of Laser Processed Fe-Cr Surface Alloys, P. A. Molian, K. H. Khan and W. E. Wood, 39th Ann. Proc. Electron Microscopy Soc. Amer., Atlanta, GA, 1981, G. W. Bailey (ed.), pp. 328-329.

Phase Transformation Studies of Laser-Processed Fe-0.2%C-Cr Surface Alloys, P. A. Molian, P. J. Wang, K. H. Khan and W. E. Wood, presented at Materials Research Society Symposium on "Rapidly Solidified Amorphous and Crystalline Alloys", Boston, MA, November 17-19, 1981. (Presentation only--no paper)

Characterization of Laser-Alloyed Hard Surfaces, W. E. Wood, J. L. Johnsen, and P. A. Molian, presented at International Conference on Metallurgical Coatings and Process Technology, San Diego, CA, April 4-9, 1982. (Presentation only--no paper)

Observations of a Grain Boundary Phase in Laser-Heat-Treated Ultrahigh Strength Low Alloy Steels, P. A. Molian, Materials Science and Engineering, 56 (3), December 1982, pp. 265-269.

Formation of Austenite in Laser-Processed Fe-0.2%C-20%Cr Alloy, P. A. Molian and W. E. Wood, Mat. Sci. & Eng., 56 (3), December 1982, pp. 271-277.

Structural Characterization of Laser-Processed Molybdenum Steel, P. A. Molian, Mat. Sci. & Eng., 58 (2), April 1983, pp. 175-180.

Recent Advances in Surface Modification Techniques, P. A. Parrish and W. E. Wood, presented at the Pacific Northwest Materials Conference, Seattle, WA, May 18, 1983. (Presentation only--no paper)

Phase Changes in a Laser Alloyed Fe-5Cr Steel, R. Padmanabhan and W. E. Wood, 41st Ann. Proc. Electron Microscopy Soc. Amer., Phoenix, AZ, August 1983, G. W. Bailey (ed.), pp. 228-229.

Transformation Behaviour of Laser Processed Fe-5%Cr, Fe-5%Ni and Fe-6%Cr-2%Ni Alloys, P. A. Molian and W. E. Wood, Journal of Materials Science, 18 (9), September 1983, pp. 2555-2562.

Transformation Structures and Strengthening Mechanisms of Laser Processed Fe-Cr Alloys, P. A. Molian and W. E. Wood, Journal of Materials Science, 18 (9), September 1983, pp. 2563-2571.

Non-equilibrium Phases in Laser-Processed Fe-0.2wt.%C-20wt.%Cr Alloys, P. A. Molian and W. E. Wood, Materials Science and Engineering, 60 (3), September 1983, pp. 241-245.

Solid State Transformation Structures of Rapidly Solidified Fe-1.0%C-Cr Steels, P. A. Molian and W. E. Wood, submitted for publication to Materials Science and Engineering.

Microstructures of Rapidly Solidified Laser Processed Fe-0.5%C-Cr Alloys, P. A. Molian and W. E. Wood, submitted for publication.

Effect of Coating Morphology on Melt Penetration Depth of Laser Surface Alloyed Iron, P. A. Molian and W. E. Wood, submitted for publication in Journal of Materials Science Letters.

LIST OF PARTICIPATING SCIENTIFIC PERSONNEL

1. W. E. Wood -- Principal Investigator, Dept. Chairman & Professor
2. P. A. Molian* -- Graduate Student Research Assistant
3. J. L. Johnsen -- Senior Research Engineer
4. D. M. Walker -- Research Engineer
5. R. Padmanabhan -- Research Scientist
6. R. B. Turpin -- Senior Research Associate

*Ph.D. Thesis Completed and Degree Awarded


FILM
3-8